7B.4 HIGH SPECTRAL RESOLUTION LAND SURFACE TEMPERATURE AND EMISSIVITY MEASUREMENT IN THE THERMAL INFRARED

Nicholas Bower*, Robert O Knuteson, Hank E Revercomb
CIMSS, SSEC, University of Wisconsin, Madison, WI USA

1 INTRODUCTION

Thermal emission from a land surface is dependent on both the spectral emissivity, an intrinsic property of the surface determined by its composition and texture, and the surface kinetic temperature. In the remote sensing of a land surface, usually neither of these properties are adequately known *a priori*, and in the ideal case where the atmosphere has been adequately characterized, there remains $N+1$ unknown quantities for only N spectral measurements. Here lies the problem of temperature/emissivity separation, which has been addressed by others such as (Gillespie et al., 1998), (Hook et al., 1992), (Kahle and Alley, 1992), (Labed and Stoll, 1991) and (Borel, 1998).

Algorithms have been in ongoing development by the Co-operative Institute for Meteorological and Satellite Studies (CIMSS) at the University of Wisconsin (UW) which involve high spectral resolution measurement on and between atmospheric emission lines (Smith et al., 1996). Under the valid assumption that surface emissivity spectra are spectrally smoother than atmospheric emission, these methods provide the extra constraint needed to address the temperature/emissivity problem. Such a method, first reported by (Xie, 1993), is shown here applied to measurements of various land surfaces made with an Atmospheric Emitted Radiance Interferometer (AERI), an instrument also developed by the UW.

2 THEORY

The thermal infrared radiance detected by a downward-looking sensor can be expressed by,

$$R(\theta,\phi) = \tau(\theta,\phi)\epsilon(\theta,\phi)B(T) \; + \; I_{sky\uparrow}(\theta,\phi) + \quad (1)$$

$$\tau(\theta,\phi)\int_0^{2\pi}\int_0^{\pi/2} f(\theta_i,\phi_i,\theta,\phi)I_{sky\downarrow}(\theta_i,\phi_i)cos\theta_i d\theta_i d\phi_i$$

where $f(\theta_i,\phi_i,\theta,\phi)$ is the bidirectional distribution function (BRDF) with units of sr^{-1} that represents the proportion of incident downwelling irradiance at (θ_i,ϕ_i) that is reflected as radiance into the direction of observation (θ,ϕ).

For a Lambertian surface, (1) may be linearized by invoking Kirchhoff's Law for an opaque body in thermodynamic equilibrium (Norman and Becker, 1995):

$$\epsilon(\theta,\phi) = 1 - \rho(\theta,\phi) \quad (2)$$

where $\rho(\theta,\phi)$ is hemispherical-directional reflectance. The validity of this approximation for angular measurement of natural surfaces measured in the field environment is currently under consideration, and is not known to have been thoroughly investigated elsewhere.

Using (2), (1) may be expressed as,

$$\epsilon(\theta,\phi) = \frac{I(\theta,\phi) - I_{sky\uparrow}(\theta,\phi) - \tau(\theta,\phi)\overline{I_{sky\downarrow}}}{\tau(\theta,\phi)(B(T_s) - \overline{I_{sky\downarrow}})} \quad (3)$$

where for a sky with azimuthal symmetry the effective average downwelling radiance $\overline{I_{sky\downarrow}}$ (basically the spectral irradiance divided by π) is given by,

$$\overline{I_{sky\downarrow}} = 2\int_0^{\pi/2} I_{sky\downarrow}(\theta_i)cos\theta_i sin\theta_i d\theta_i \quad (4)$$

For a ground based instrument with a negligable ground-sensor path radiance and near-unity transmittance,

$$\epsilon(\theta,\phi) = \frac{I(\theta,\phi) - \overline{I_{sky\downarrow}}}{B(T_s) - \overline{I_{sky\downarrow}}} \quad (5)$$

After the required directional measurements of $I(\theta,\phi)$ and $I_{sky\downarrow}(\theta_i,\phi_i)$ are made with AERI, equation 5 still requires the surface temperature T in order to calculate the directional spectral emissivity $\epsilon(\theta,\phi)$. This simultaneous separation of two quantities from a single measurement of $I(\theta,\phi)$ is approached by acknowledging that surface emission is spectrally smoother than atmospheric emission. By guess and subsequent refinement of the surface temperature in equation 5, the surface emissivity is dervied when surface-reflected atmospheric radiance emission lines in the upwelling radiance $I(\theta,\phi)$ are effectively *balanced* with the emission lines in the downwelling atmospheric radiance $\overline{I_{sky\downarrow}}$ (according to the assumed reflection of (2)). In effect, the surface temperature producing the maximum smoothness, characteristic of a land surface emissivity

* *Corresponding author address:* Nicholas Bower, Cooperative Institute for Meteorological Satellite Studies, University of Wisconsin—Madison, email:nick.bower@ssec.wisc.edu

spectrum, is desired with maximal removal of sharp atmospheric emission lines through indirect optimization of the amount of surface reflection.

The process of surface temperature refinement to obtain maximum smoothness in directional spectral emissivity is shown in Figure 1.

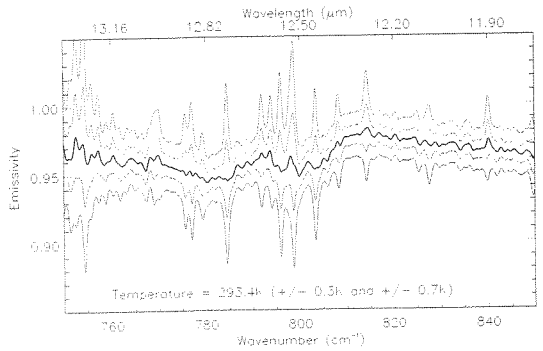

Figure 1: Derived surface emissivities with variation of temperature estimate. The optimum temperature is obtained when the calculated emissivity has maximum smoothness, devoid of narrow atmospheric emission spectral lines

This procedure has been implemented by minimization of the average squared derivative with wavenumber of the 757–782 cm^{-1}spectral region. This region contains a mixture of CO_2 and H_2O emission lines which are strong enough to provide adequate sensitivity yet not too strong to be greatly affected by surface-sensor transmission or be derived from such a short path length that the surface-atmosphere temperature difference is small.

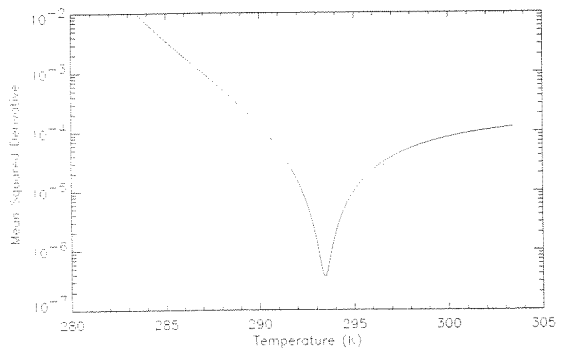

Figure 2: Mean squared derivative indicator of surface temperature. Best estimate where the curve is minimized

The accuracy by which temperature and emissivity can be retrieved is dependent on the degree to which the angular approximation (2) holds and instrument radiometric accuracy. The authors feel that better than 0.01 emissivity and 0.5K temperature accuracy is being achieved for the presented measurements. Further measurements and comprehensive error and sensitivity analyses are required to further understanding of the method. The bidirectional reflectance of soils however makes realistic simulations difficult and so field measurements of emissivity and temperature controlled standards may also be pursued.

3 INSTRUMENTATION

The University of Wisconsin has an Atmospheric Emitted Radiance Interferometer (AERI) instrument installed in a mobile vehicle. The AERI obtains a spectrum of calibrated radiance (100 s dwell) over the spectral range 3.3–18 μm at a spectral resolution of 0.5 cm^{-1}(unapodized). The calibrated radiance has a noise equivalent radiance of better than 0.2 $mW/(m^2\ sr\ cm^{-1})$ in the 8–12 μm region and better than 0.015 $mW/(m^2\ sr\ cm^{-1})$ in the 4–5 μm region. The instrument field of view is a two inch beam which diverges with a full angle of 1.7 degrees. When extended vertically with a hydraulic ram (16 feet) the field of view spot size at ground level at an angle of 45 degrees is about 11–12 inches in diameter.

4 DATA ANALYSIS AND RESULTS

Results are presented from two measurement periods in December at Edwards AFB and January at the Salton Sea, both in Southern California.

4.1 Results from a Diffuse Isothermal Surface

AERI measurements were made during a MASTER validation flight at the Salton Sea, January 16–18th 1999. On the flight day (17th), an asphalt parking lot was selected for emissivity measurement. It's surface was dark blue and covered with half-centimeter loose rocks. The surface appeared visibily homogeneous, and made an excellent candidate for future comparison of AERI and larger footprint MASTER thermal measurements. AERI measurements were made of the surface at 45, 60 and 70 degrees from nadir, and sky measurements were made at zenith, 45, 60 and 75 degrees. Derived surface temperatures and emissivities using the presented algorithm are shown in the following figures.

Figure 3 shows three angular downward-looking measurements, each using a single sky view to calculate emissivity. Excellent agreement of the calculated surface temperature exists between the three angular surface measurements. The increase in spectral contrast with angle is probably due to a small overall specular component to the surface reflectance . The emissivity signature is predictably that of the mineral quartz.

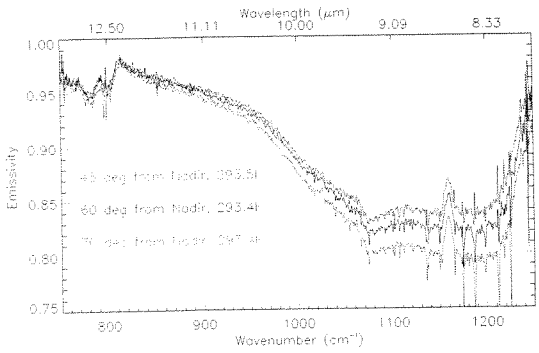

Figure 3: Derived surface temperature and emissivity for asphalt parking lot for 45, 60 and 70 degree surface views. Single 60 degree sky measurement used in all cases.

Figure 4 shows the effect of using different sky view angles for a single downward-looking measurement. It is seen that the derived surface temperature is relatively unaffected by the choice of angular sky measurement used in the calculation. Although somewhat surprising, this is encouraging for the potential of the 757–782 cm^{-1}spectral window used. This invariability with sky angle effect was also seen in measurements of nearby sandy desert terrain, but was not seen using other spectral windows with the same data, or in the other measurements of clay playas presented later. It is very possible that the surface texture (roughness or grain size relative to wavelength) is responsible for this and influences how much specular component exists in the surface reflectance.

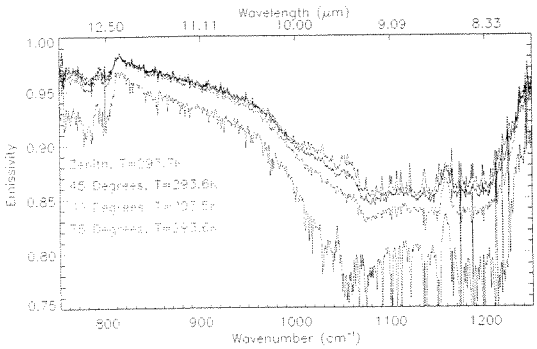

Figure 4: Derived surface temperature and emissivity using a single surface view of 60 degrees and each of 4 different sky views (0, 45, 60 and 75 degrees)

4.2 Rodgers Dry Lake

The AERI was deployed to Edwards AFB on December 17–22, 1998 for surface emissivity validation of MODIS Airborne Scanner (MAS) flights aboard a NASA ER-2. Lake Rodgers, a clay playa, was used as the land surface validation target. Figure 5 shows the derived surface temperature using equation 5 during a 3 hour period of pre-sunrise to mid-morning heating for 45 and 60 degree surface views. Following this are the first and final emissivities for each of the two surface angles from this measurement period.

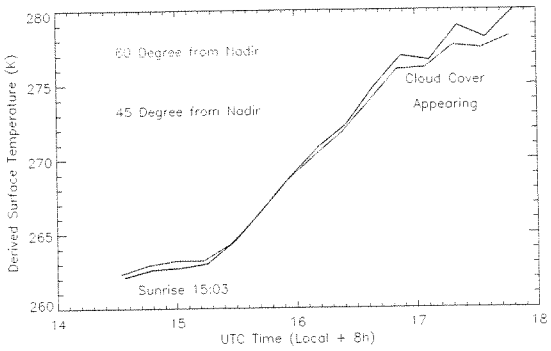

Figure 5: Derived surface temperature at Lake Rodgers on December 21st 1998 beginning before sunrise and ending mid-morning for view angles of 45 and 60 degrees from nadir. 60 degree upward-looking measurement used for $\overline{I_{sky\downarrow}}$

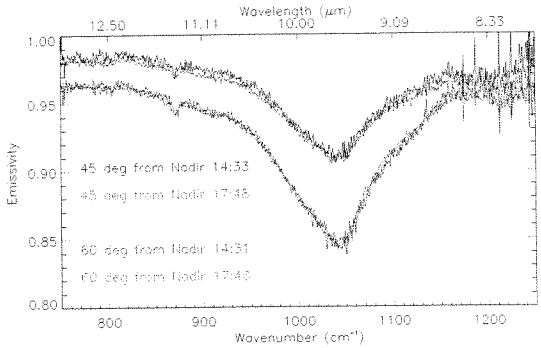

Figure 6: Derived surface emissivities for 45 and 60 degree view angles at Lake Rodgers for start and end of the period shown above

Close agreement for each of the observation angles exists in Figure 6 between pre-sunrise and mid-morning, which shown by Figure 5 to be separated by approximately 15 K. This shows; 1) independence of the derived emissivity using the presented algorithm to the surface temperature for the surface measured, and 2) no detectable surface moisture transport which would change the emissivity (Salisbury and D'Aria, 1992). Apart from the extensive cracking of the clay surface, the playa showed larger scale visible inhomogenaety

with two main surface types being either a brown clay or a white clay. It is felt that some of this inhomogenaety in either composition or surface texture exists between the two surface view angles has lead to an apparent difference in the two heating rates of Figure 5. Towards the end of measurement period, high level cirrus clouds started to appear and became relatively thick. The consistent agreement of each of the directional emissivities even after this points to the erratic variation of surface temperature during this time to be caused by variations in solar heating, thus providing more evidence for different thermal inertias of the two surface patches viewed.

4.3 Playa Surface Composition

With the intention of better characterizing the playa white/brown inhomogenaety, further measurements were made of another nearby playa, Lake Rosamond, on January 14th, 1999. A white and brown surface area were chosen and the calculated emissivity spectra are shown in Figure 7. Included in this figure are emissivity spectra calculated from laboratory measurements of directional-hemispherical reflectance from the ASTER Spectral Library (ASTER, 1998) of minerals with similar absorption features in their signatures.

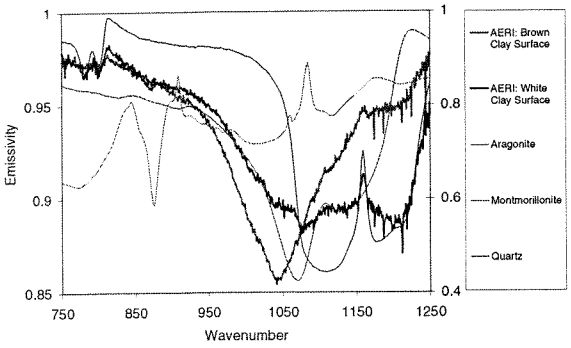

Figure 7: AERI emissivities from Lake Rosamond and several minerals with matching absorption features. Note that the high-contrast quartz emissivity is plotted on the secondary axis for comparison.

The emissivity spectrum of the white area of the playa is characteristic of the mineral quartz, a tectosilicate. Tectosilicates constitute the largest and most important of the six structural subdivisions among the silicates. The SiO_4 molecular groups of this series form a continuous three-dimensional framework. Quartz shows a primary doublet centered on 1159 $cm^{-1}$and a secondary doublet centered on 794 cm^{-1}.

The emissivity spectrum of the brown area has the following features: 1) a main absorption feature at 1046 cm^{-1}(9.56 μm), 2) a weaker feature at 873 cm^{-1} (11.45 μm) and 3) a peak at 1159 cm^{-1}(8.63 μm) and a broad dip around 1200 cm^{-1}(8.33 μm). The first feature is similar to the spectrum of montmorillonite (a member of the montmorillonite group that includes montmorillonite, nontronite, saponite and hectorite. The members of the montmorillonite group are phyllosilicates with sheet structures. However, the main montmorillonite feature is displaced to longer wavelengths. This may be due to substitution in the mineral lattice or a mixed layer clay may be present (Hook, 1999). The second feature at 873 $cm^{-1}$is characteristic of a carbonate mineral, such as shown by aragonite. The third set of features is typical of quartz.

REFERENCES

ASTER. ASTER Spectral Library. http://speclib.jpl.nasa.gov, 1998.

Borel, C. C. (1998): Surface Emissivity and Temperature Retrieval for a Hyperspectral Sensor. In *1998 IEEE International Geoscience and Remote Sensing Symposium Proceedings.*

Gillespie, A., Rokugawa, S., Matsunaga, T., Cothern, J. S., Hook, S., and Kahle, A. B. (1998): A Temperature and Emissivity Separation Algorithm for Advanced Spaceborne Thermal Emission and Reflection Radiometer (ASTER) Images. *IEEE Transactions on Geoscience and Remote Sensing*, **36**, pp. 1113–1126.

Hook, S. Personal Communication, 1999.

Hook, S. J., Gabell, A. R., Green, A. A., and Kealy, P. S. (1992): A comparison of Techniques for Extracting Emissivity Information from Thermal Infrared Data for Geologic Studies. *Remote Sensing of the Environment*, **42**, pp. 123–135.

Kahle, A. B. and Alley, R. E. (1992): Separation of Temperature and Emittance in Remotely Sensed Radiance Measurements. *Remote Sensing of the Environment*, **42**, pp. 107–111.

Labed, J. and Stoll, M. P. (1991): Angular Variation of Land Surface Emissivity in the Thermal Infrared: Laboratory Investigations on Bare Soils. *International Journal of Remote Sensing*, **12**, pp. 2299–2310.

Norman, J. M. and Becker, F. (1995): Terminology in Thermal Infrared Remote Sensing of Natural Surfaces. *Agricultural and Forest Meteorology*, **77**, pp. 153–166.

Salisbury, J. W. and D'Aria, D. M. (1992): Infrared (8–14 μm) Remote Sensing of Soil Particle Size. *Remote Sensing of the Environment*, **42**, pp. 157–165.

Smith, W. L., Knuteson, R. O., Revercomb, H. E., et al. (1996): Observations of the Infrared Radiative Properties of the Ocean — Implications for the Measurements of Sea Surface Temperature via Satellite Remote Sensing. *Bulletin of the American Meteorological Society*, **77**, pp. 41–51.

Xie, R. (1993): Retrieving Surface Temperature and Emissivity from High Spectral Resolution Radiance Observations. Master's thesis, Atmospheric Sciences, University of Wisconsin-Madison.